

## RESEARCH ARTICLE

# Performance comparison of structured $\mathcal{H}_\infty$ based looptune and LQR for a 4-DOF robotic manipulator

Arafat Asghar<sup>1</sup>, Muhammad Iqbal<sup>2</sup>, Abdul Khaliq<sup>3</sup>, Saif ur Rehman<sup>4</sup>, Jamshed Iqbal<sup>5\*</sup>

**1** High Voltage and Short Circuit Laboratory, National Transmission and Despatch Company (NTDC), Rawat, Islamabad, Pakistan, **2** Department of Computer Science, National University of Technology (NUTECH), Islamabad, Pakistan, **3** Department of Electrical and Computer Engineering, Sir Syed CASE Institute of Technology, Islamabad, Pakistan, **4** Department of Electrical Engineering, Superior University, Lahore, Pakistan, **5** Department of Computer Science and Technology, Faculty of Science and Engineering, University of Hull, Hull, United Kingdom

\* [j.iqbal@hull.ac.uk](mailto:j.iqbal@hull.ac.uk)

## Abstract

We explore `looptune`, a MATLAB-based structured  $\mathcal{H}_\infty$  synthesis technique in the context of robotics. Position control of a 4 Degree of Freedom (DOF) serial robotic manipulator developed using Simulink is the problem under consideration. Three full state feedback control systems were developed, analyzed and compared for both steady-state and transient performance using the Linear Quadratic Regulator (LQR) and `looptune`. Initially, a single gain feedback controller was synthesized using LQR. This system was then modified by augmenting the state feedback controller with Proportional Integral (PI) and Integral regulators, thereby creating a second and third control system respectively. In both the second and third control systems, the LQR synthesized gain and additional gains were further tuned using `looptune` to achieve improvement in performance. The second and third systems were also compared in terms of tracking a time-dependent trajectory. Finally, the LQR and `looptune` synthesized controllers were tested for robustness by simultaneously increasing the mass of each manipulator link. In comparison to LQR, the second system consisting of Single Input Single Output (SISO) PI controllers and the state feedback matrix succeeded in meeting the control objectives in terms of performance, optimality, trajectory tracking, and robustness. The third system did not improve performance in contrast to LQR, but still showed robustness under mass variation. In conclusion, our results have shown `looptune` to have a comparatively better performance over LQR thereby highlighting its promising potential for future emerging control system applications.

## OPEN ACCESS

**Citation:** Asghar A, Iqbal M, Khaliq A, Rehman Su, Iqbal J (2022) Performance comparison of structured  $H_\infty$  based looptune and LQR for a 4-DOF robotic manipulator. PLoS ONE 17(4): e0266728. <https://doi.org/10.1371/journal.pone.0266728>

**Editor:** Qichun Zhang, University of Bradford, UNITED KINGDOM

**Received:** February 8, 2022

**Accepted:** March 28, 2022

**Published:** April 11, 2022

**Copyright:** © 2022 Asghar et al. This is an open access article distributed under the terms of the [Creative Commons Attribution License](https://creativecommons.org/licenses/by/4.0/), which permits unrestricted use, distribution, and reproduction in any medium, provided the original author and source are credited.

**Data Availability Statement:** All relevant data are within the manuscript.

**Funding:** The author(s) received no specific funding for this work.

**Competing interests:** The authors have declared that no competing interests exist.

## 1 Introduction

Current research in robotics is focused on devising novel solutions for a variety of control problems [1] such as executing motion in deformable and uneven spaces, gripping delicate and fragile objects, performing efficient supervisory control for swarm robots etc. These tasks

become critically important in the context of human-robot interaction [2]. “Anthropocentric” or “human-friendly” intelligent robotic systems are gradually becoming ubiquitous. However, researchers are confronted by the highly nonlinear, random, and time-varying nature of the control problems [3, 4]. As reported in several works [2, 5–15], adaptive, intelligent and robust control techniques are one of the many strategies having potential to overcome the above-mentioned problems.

Adaptive control algorithms incorporate parameter estimation in one form or the other [16] and is further classified into conventional and robust categories [17]. Although adaptive control demonstrably achieves continuous improvement in tracking error, assumptions on structure and uncertainty size are made in most of the methods. Also, several studies have proven “model-free” or no “prior assumptions on the plant” controllers to exhibit poor performance [18–21]. Intelligent control is the application of artificial or computer-aided intelligence techniques such as neural networks, evolutionary computation, fuzzy logic [22], machine or reinforcement learning to (usually) complex and non-trivial dynamical systems [23, 24]. In [25], a full-state output-feedback adaptive fuzzy controller has been devised with output constraint. Likewise, an adaptive impedance-based control strategy using neural networks was developed to tackle dynamical uncertainties dynamics for a trajectory tracking problem [26]. Although the future of intelligent control seems promising [27, 28], the cost and failure rate associated with implementing such control schemes is higher in comparison to conventional schemes, especially for complex systems. Moreover, artificial neural network-based control designs are mostly simulation-based with slight evidence of practical implementation [2].

In robust control, a pre-designed static or fixed structure controller compensates for bounded parametric uncertainties or disturbances and therefore does not require online tuning [29, 30]. Thus, robust control offers better performance in terms of responsiveness [31] and practical realization [32] in comparison to adaptive control. An overview of robust control for robotic manipulators has been presented in [33–35].  $\mathcal{H}_\infty$  control is a well-known robust control technique and has been applied extensively on a variety of rigid and flexible robotic models. Control design for a quadcopter has been developed by integrating nonlinear  $\mathcal{H}_\infty$  and Model Predictive Control [36] and in [37] by using integral sliding mode control. A robust regulator was designed for a 2 Degree Of Freedom (DOF) platform using mixed  $\mathcal{H}_2/\mathcal{H}_\infty$  synthesis and considering pole-placement constraints in a linear matrix inequality framework [38].  $\mathcal{H}_\infty$  regulation using local gravitational force compensation for a 3-DOF robotic manipulator was designed in [39]. In [40], a finite-time globally stable  $\mathcal{H}_\infty$  controller was designed without solving for Hamilton-Jacobi equation or Algebraic Riccati equation by using the backstepping method. Luo et al. devised  $\mathcal{H}_\infty$  control for 2-Dimensional (2D) Takagi–Sugeno fuzzy systems characterized by time-delays and missing measurements within a second Fornasini–Machesini local state-space framework [41]. Similarly, a novel 2D sensor state estimator guaranteeing  $l_2$ - $l_\infty$  disturbance attenuation and power bound constraints has been developed in [42]. In [43], a novel nonlinear  $\mathcal{H}_\infty$  controller has been designed for a multi-DOF robotic arm using the concept of min-max differential games. An adaptive fuzzy neural network controller based on impedance learning was implemented for a constrained 3-DOF robot in [44]. The idea of inverse optimal Proportional Integral Derivative (PID) control combined with Feed-Forward control in an  $\mathcal{H}_\infty$  framework has been considered in [45]. Finally,  $\mathcal{H}_\infty$  control has been designed for distributed/decentralized control using multiple industrial manipulators [46].

In all of the methods described above, a centralized and full-order controller is obtained without the possibility of enforcing structure. The controllers are synthesized by either Semi

Definite Programming (SDP) [47], Algebraic Riccati Equations [48] or bounded real lemmas involving Lyapunov variables. Structural constraints cause Bilinear Matrix Inequalities (BMIs) to be introduced into such  $\mathcal{H}_\infty$  techniques and make them non-convex. Optimization programs of moderate size have been proven to experience numerical complications for such BMIs [49].

The development of novel nonsmooth optimization techniques has allowed for structured  $\mathcal{H}_\infty$  synthesis to be carried out under structural constraints [49, 50]. These algorithms were finally incorporated in MATLAB [51–53] as `hinfstruct` and `looptune` commands in the Robust Control Toolbox. While `hinfstruct` has been successfully applied in several control studies [54–63], it requires the design requirements to be specified in terms of a well-posed  $\mathcal{H}_\infty$  optimization problem. However, strong scaling and tight coupling in multi-loop control systems may lead to ill-posing of the  $\mathcal{H}_\infty$  problem. Erroneous results may also arise due to cross-coupling between feedback loops when considering stability margins of each loop separately [64, 65]. Finally, in the studies described above no comparison of `hinfstruct` with existing control techniques in literature or improvement thereof has been considered.

On the other hand, the `looptune` command allows the user to specify the  $\mathcal{H}_\infty$  problem in terms of generalized high-level requirements, which lead to satisfactory results despite the problems described above [51, 53]. The `looptune` command has been used to tune a 2-DOF PID controller which is then augmented with a reset controller for a 4-DOF robotic arm [66]. In [67], adaptive control is augmented with a `looptune/hinfstruct` synthesized robust controller. Zhao et al. developed a multi-variable robust controller for an electrified turbo-charger using `looptune` [68]. Finally, in [69] `looptune` has been used to develop an outer control loop for a flexible x-hale aircraft, in conjunction with Gain Scheduling [70].

This study has been specifically conducted to assess the advantage of the novel MATLAB command `looptune`. For this purpose, comparison with a well-known optimal control technique, namely the Linear Quadratic Regulator (LQR) is carried out. The control problem under consideration is position control of a 4-DOF robotic arm developed in SimMechanics/Simulink. With LQR, only a single gain can be synthesized for state feedback control. Determination of the optimum solution to the Algebraic Riccati Equation in LQR is often a tedious and time-consuming process. Finally, LQR does not provide robustness against uncertainties or disturbances. On the other hand, `looptune` allows minimization of the  $\mathcal{H}_\infty$  norm by tuning gains, transfer functions, state space models etc. in the control loop. Therefore, state feedback control can be modified to achieve optimal and robust performance.

To determine whether this is indeed the case, we developed two novel state feedback controllers by supplementing the original state feedback gain with additional gains, thus forming two different versions of PI control. Owing to its simplicity and ease of implementation, PI/PID control is the most widely used control algorithm [71]. For the first controller, Single Input Single Output (SISO) PI controllers were added. In the second controller, a Multi-Input Multi-Output (MIMO) gain and integrator was added to form a MIMO PI controller. The `looptune` synthesized controllers were then compared against each other and the LQR synthesized single gain controller. As of present, no research article has compared the performance of `looptune` to LQR or other control techniques, especially in the context of position control for a 4-DOF robotic manipulator. The main contributions of this paper can be summarized as follows:

1. Development of two novel state feedback controllers by modifying the original single gain state feedback controller.
2. Tuning the gains of the novel state feedback controllers to achieve the desired specification.

3. Comparison of LQR and `looptune` synthesized controllers in terms of transient and steady-state performance, and robustness to uncertainty.
4. Comparison of two `looptune` synthesized controllers for trajectory tracking.
5. Using the results of the comparison to justify superiority of `looptune` over LQR in terms of performance and robustness.
6. Demonstrating the `looptune` synthesized second control system consisting of Single Input Single Output (SISO) Proportional Integral (PI) controllers and state feedback matrix as the candidate controller on a comparative basis.

The remainder of this paper is structured as follows. Section 2 describes the mathematical model of the robotic arm, while details on the performance specification, controller design and trajectory tracking are presented in Section 3. Simulation results are analyzed and discussed in Section 4. In Section 5, each of the controllers is analyzed for robustness under uncertainty. Lastly, Section 6 describes the controller selection in terms of the best overall performance and concludes the entire paper.

## 2 Model description

The robotic arm used for this research is a modification of an 8-DOF arm developed using SimMechanics in MATLAB 2012a for demonstration purposes by MathWorks. It originally consisted of five links namely the base, upper arm, forearm, wrist and gripper assembly. The base and upper arm were linked together using a 3-DOF spherical joint, while the upper arm-forearm, forearm-wrist, and wrist-gripper assembly were all linked together by 1-DOF revolute joints. Finally, the gripper assembly was composed of two fingers each having 1-DOF.

For our research, the gripper assembly was removed and the spherical joint was replaced by 2-DOF universal joint. The rest of the manipulator structure was kept intact. This modification resulted in a 4-DOF robotic manipulator which is more or less similar to many commercially available robotic manipulators. [Fig 1](#) shows a basic sketch of the manipulator outlining its overall structure, home configuration and initial conditions. The initial conditions of the manipulator are given as  $\theta_1 = 0$ ,  $\theta_2 = 0$ ,  $\theta_3 = 0$  and  $\theta_4 = 0$ .

[Fig 2](#) shows the implementation of the robotic arm in SimMechanics, a multibody toolbox in Simulink/MATLAB used for simulation and modeling of mechanical and electro-mechanical systems. The “Body Block” represents an individual robotic arm link such as the base, forearm, upper arm, and wrist. The “Universal/Revolute Joint Block” and “Weld Joint Block” determine rotation and fixation between two robotic arm links respectively. Actuation of the joints is provided by the “Joint Actuator Block”, while output from the joint is obtained using “Joint Sensor Block”. The “Ground Block”, is an immobile ground point relative to an absolute inertial reference frame. Finally, the “Environment Block” is used for configuration of the simulation. The simulations have been performed on an Intel Core i5-2450M CPU system with 8 GB RAM and 500 GB Hard Disk. [Table 1](#) describes the physical parameters of the SimMechanics model of the Manipulator.

As seen in [Fig 1](#), each joint has been assigned a number along with its respective angle. Each joint axis orientation is given in the adjacent parenthesis. Using MATLAB’s “Linear Analysis Toolbox”, the robotic manipulator is linearized about the initial conditions given in [Fig 1](#), inputs A, B, C and D, and outputs E, F, G, H, I, J, K, and L given in [Fig 2](#). This results in a linear state space model. The dynamic equation of motion for a robotic manipulator is

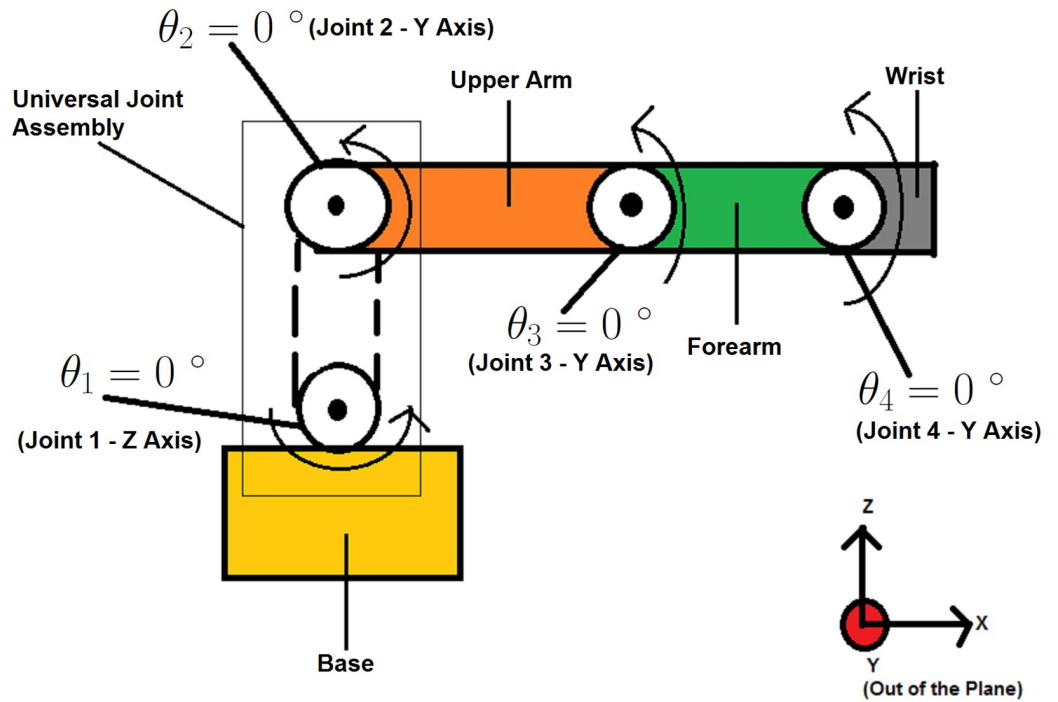


**Fig 1. Home configuration of the robotic manipulator.**

<https://doi.org/10.1371/journal.pone.0266728.g001>

given in (1).

$$\tau = M(\theta)(\ddot{\theta}) + V(\theta, \dot{\theta}) + G(\theta) \tag{1}$$

$M(\theta)$  is a positive definite inertia matrix,  $V(\theta, \dot{\theta})$  is a vector representing centrifugal and Coriolis forces,  $G(\theta)$  is a vector for denoting gravitational forces and is a vector representing actuator torques. Deriving the above equations manually using Euler-Lagrange or Euler-Newton methodology is a tedious and lengthy procedure. SimMechanics allows for simulation and linear analysis of the robot dynamics without the need to derive (1).

The system described above has 8 states, 4 inputs and 8 outputs. The joints have been indexed as  $i = 1, 2, 3, 4$  according to the configuration shown in Fig 1. The variables  $\theta_i, \dot{\theta}_i, \ddot{\theta}_i$

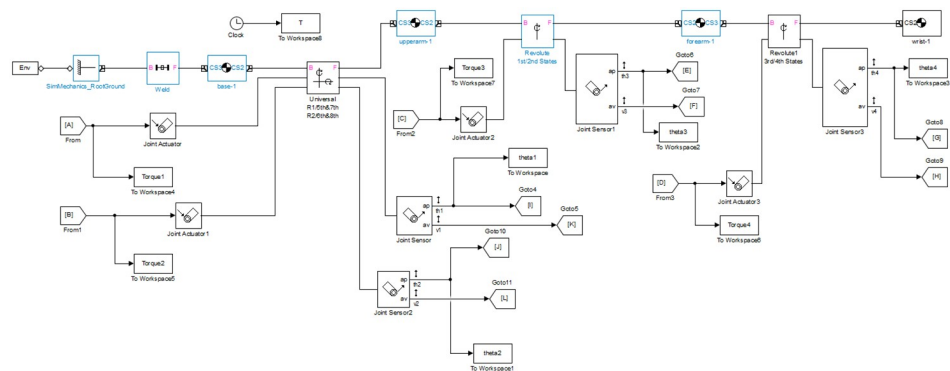


**Fig 2. Simulink open-loop model of the robotic manipulator.**

<https://doi.org/10.1371/journal.pone.0266728.g002>

Table 1. Physical parameters of the SimMechanics/Simulink model.

Link	Mass(kg)	Length(m)	Moment of Inertia Tensor( $kg.m^2$ )
Base	9.465	0.1328	$\begin{bmatrix} 0.0198 & 0.0003 & 0.0000 \\ 0.0003 & 0.0401 & 0.0000 \\ 0.0000 & 0.0000 & 0.0274 \end{bmatrix}$
Upper Arm	0.8016	0.1003	$\begin{bmatrix} 0.0007 & -0.0001 & 0.0000 \\ -0.0001 & 0.0025 & 0.0000 \\ 0.0000 & 0.0000 & 0.0024 \end{bmatrix}$
Forearm	1.005	0.1092	$\begin{bmatrix} 0.0007 & -0.0001 & 0.0000 \\ -0.0001 & 0.0025 & 0.0000 \\ 0.0000 & 0.0000 & 0.0024 \end{bmatrix}$
Wrist	0.1517	0.0305	$1e - 4 \times \begin{bmatrix} 0.2711 & -0.0000 & -0.0000 \\ -0.0000 & 0.4630 & 0.0000 \\ -0.0000 & 0.0000 & 0.3879 \end{bmatrix}$

<https://doi.org/10.1371/journal.pone.0266728.t001>

and  $\tau_i$  represent the angular position/displacement, angular velocity, angular acceleration and applied torque/actuation of the  $i^{th}$  joint respectively.

### 3 Controller design

#### 3.1 Linear quadratic regulator

The control design strategy has been formulated with the performance specification outlined in Table 2. Since our focus is on position control only, a system with Type I steady-state error is proposed. For Type I systems, the steady-state error for a step input (position constant) is zero, finite for a ramp input (velocity constant) and infinite for a parabolic input (acceleration constant) [72].

The Q and R matrices are the state and control weighting matrices respectively and are shown below by (2) and (3):

$$Q = \begin{bmatrix} \theta_3 & 0 & 0 & 0 & 0 & 0 & 0 & 0 \\ 0 & \dot{\theta}_3 & 0 & 0 & 0 & 0 & 0 & 0 \\ 0 & 0 & \theta_4 & 0 & 0 & 0 & 0 & 0 \\ 0 & 0 & 0 & \dot{\theta}_4 & 0 & 0 & 0 & 0 \\ 0 & 0 & 0 & 0 & \theta_1 & 0 & 0 & 0 \\ 0 & 0 & 0 & 0 & 0 & \theta_2 & 0 & 0 \\ 0 & 0 & 0 & 0 & 0 & 0 & \dot{\theta}_1 & 0 \\ 0 & 0 & 0 & 0 & 0 & 0 & 0 & \dot{\theta}_2 \end{bmatrix} \tag{2}$$

Table 2. Specification of the proposed control system.

S. No	Parameters	Allowed Limit
1	Rise Time	3 seconds
2	Settling Time	6 seconds
3	Steady-State Error	10%
4	Maximum Peak Torque	$\pm 130$ Nm
5	Overshoot and Undershoot	15%

<https://doi.org/10.1371/journal.pone.0266728.t002>

$$R = \begin{bmatrix} \tau_1 & 0 & 0 & 0 \\ 0 & \tau_2 & 0 & 0 \\ 0 & 0 & \tau_3 & 0 \\ 0 & 0 & 0 & \tau_4 \end{bmatrix} \tag{3}$$

Eqs (2) and (3) are then used to solve the Algebraic Riccati Equation given as follows in (4):

$$A^T X + XA - XBR^{-1}B^T X + Q = 0 \tag{4}$$

Where **A** represents the state matrix, **B** is the control input matrix, and **X** is a solution to the above equation. By substituting **X** into (5), the control law  $\tau$  is obtained as under.

$$\tau = -R^{-1}B^T Xx = -K_{QR}x \tag{5}$$

Here  $K_{LQR}$  represents the gain calculated using the LQR algorithm, while  $x = [\theta_3 \ \dot{\theta}_3 \ \theta_4 \ \dot{\theta}_4 \ \theta_1 \ \theta_2 \ \dot{\theta}_1 \ \dot{\theta}_2]^T$  denotes the state vector of the system.

Fig 3 shows the implementation of the control scheme in Simulink. Outputs from the sensor blocks are multiplexed into a single signal and then subtracted from the signal emanating from the reference “Constant Block”. The difference or error signal is then fed to state feedback gain represented by the “Gain Block”.

Next, a quantity  $\tilde{x}$  is defined in (6) to denote the error or deviation from the reference or desired signal **r**. Using (6), closed loop dynamical model of the system is represented in (7).

$$\tilde{x} = r - x \tag{6}$$

$$\dot{\tilde{x}} = (A - BK_{LQR})\tilde{x} - Ar \tag{7}$$

### 3.2 Control cases

Using the idea presented in [73], two cases of initial and final positions have been considered to check whether controller performance is adversely affected by change of initial or final conditions. The first case represents the home configuration of the robotic arm, therefore the initial conditions in this configuration are zero by default. In the second set, all initial conditions have been set to 35 degrees. The initial condition for the second set is the final position of the first set, while the final position for the second set is obtained by adding 35 degrees. The joints of many commercially available robotic manipulators are capable of executing such a motion [74–76]. As shown in the following sections, each of the controllers is insensitive to change in initial and final conditions.

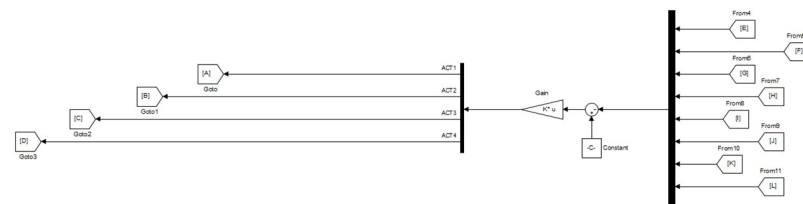


Fig 3. LQR state feedback control in Simulink.

<https://doi.org/10.1371/journal.pone.0266728.g003>

### 3.2.1 Case-1.

$$\theta_{INITIAL} = \begin{bmatrix} 0 \\ 0 \\ 0 \\ 0 \end{bmatrix}$$

$$\theta_{FINAL} = \begin{bmatrix} 35 \\ 35 \\ 35 \\ 35 \end{bmatrix}$$

### 3.2.2 Case-2.

$$\theta_{INITIAL} = \begin{bmatrix} 35 \\ 35 \\ 35 \\ 35 \end{bmatrix}$$

$$\theta_{FINAL} = \begin{bmatrix} 70 \\ 70 \\ 70 \\ 70 \end{bmatrix}$$

## 3.3 Manual tuning

In this procedure, the weights or values of  $\theta_1, \theta_2, \theta_3$  and  $\theta_4$  inside the cost matrix  $\mathbf{Q}$  are adjusted while keeping the values of  $\dot{\theta}_1, \dot{\theta}_2, \dot{\theta}_3$  and  $\dot{\theta}_4$  constant at 1, until the performance objectives specified in Table 2 have been achieved. Likewise, the values of  $\tau_1, \tau_2, \tau_3$  and  $\tau_4$  inside the matrix  $\mathbf{R}$  are kept constant at 1. The final  $\mathbf{Q}$  and  $\mathbf{R}$  matrices obtained are shown respectively in (8) and (9).

$$\mathbf{Q} = \begin{bmatrix} 10 & 0 & 0 & 0 & 0 & 0 & 0 & 0 \\ 0 & 1 & 0 & 0 & 0 & 0 & 0 & 0 \\ 0 & 0 & 10 & 0 & 0 & 0 & 0 & 0 \\ 0 & 0 & 0 & 1 & 0 & 0 & 0 & 0 \\ 0 & 0 & 0 & 0 & 10 & 0 & 0 & 0 \\ 0 & 0 & 0 & 0 & 0 & 10 & 0 & 0 \\ 0 & 0 & 0 & 0 & 0 & 0 & 1 & 0 \\ 0 & 0 & 0 & 0 & 0 & 0 & 0 & 1 \end{bmatrix} \quad (8)$$

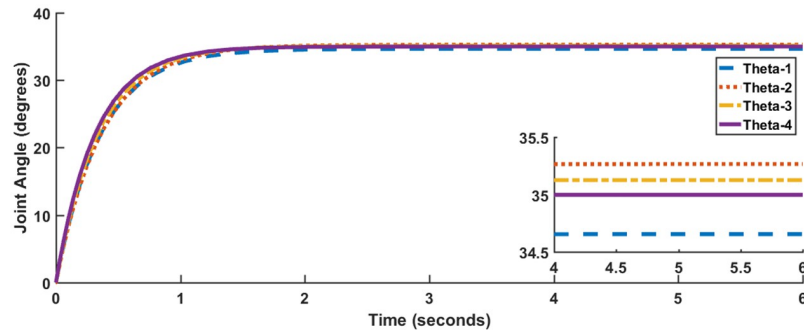


Fig 4. Response for LQR, Case I.

<https://doi.org/10.1371/journal.pone.0266728.g004>

$$R = \begin{bmatrix} 1 & 0 & 0 & 0 \\ 0 & 1 & 0 & 0 \\ 0 & 0 & 1 & 0 \\ 0 & 0 & 0 & 1 \end{bmatrix} \tag{9}$$

Substituting (8) and (9) into (4), and then substituting the result into (5), gives the value of the state feedback gain shown by (10).

Fig 4 shows the response of all four joint angles, while Fig 5 shows the response of actuator torques. The timescale in Fig 5 has been compressed to 10 milliseconds for better visibility. The responses satisfy the performance specification criteria enlisted in Table 1. However, all of the joint angles excluding  $\theta_4$  suffer from a slight steady-state error. Also, each of the actuator torque exceeds 100 Nm.

$$K_{LQR} = \begin{bmatrix} 0.0000 & 0.0000 & 0.0000 & 0.0012 & 3.1736 & 0.0000 & 1.1091 & 0.0000 \\ -0.0037 & 0.0422 & 0.0000 & 0.0000 & 0.0000 & 3.1596 & 0.0000 & 1.1084 \\ 3.1584 & 1.0199 & 0.0000 & 0.0000 & -0.0000 & -0.0041 & 0.0000 & 0.0421 \\ 0.0000 & -0.0000 & 3.1622 & 1.0002 & -0.0000 & -0.0000 & 0.0012 & -0.0000 \end{bmatrix} \tag{10}$$

Table 3 summarizes the results of the manually tuned LQR controller for Case I and Case II. The results of Case I and Case II are similar as far as the values of settling time, rise time

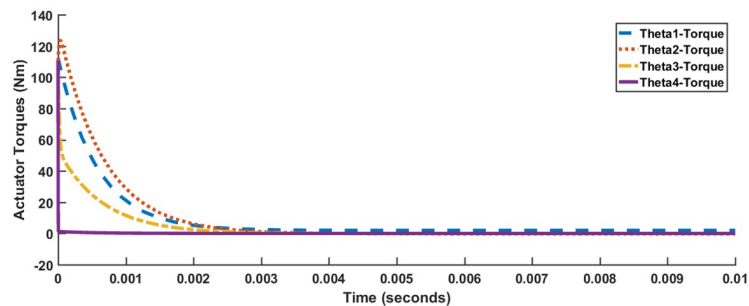


Fig 5. Actuator torques for LQR, Case I.

<https://doi.org/10.1371/journal.pone.0266728.g005>

Table 3. Summary of results for LQR.

Case	$\theta_I$	$\theta_F$	Overshoot (%)	Undershoot (%)	Settling Time (s)	Rise Time(s)	Peak Absolute Torque (Nm)	Steady-State Error (%)
I	0	35	0	0	1.3837	0.7821	111.7619	0.9866
	0	35	0	0.003265	1.4361	0.8190	123.5421	0.7568
	0	35	0	0	1.3328	0.7447	110.3999	0.3579
	0	35	0	0	1.2360	0.6978	110.6765	0.008096
II	35	70	0.0001391	0	1.3786	0.7724	111.4552	0.02858
	35	70	0.0001647	0	1.4275	0.8020	119.4106	0.7357
	35	70	0.00007223	0	1.3104	0.7403	110.3999	0.1973
	35	70	0.00002047	0	1.2463	0.6972	110.6761	0.005756

<https://doi.org/10.1371/journal.pone.0266728.t003>

and peak absolute are concerned, varying by 3% at the most. The values of overshoot, undershoot and steady-state error, although different, are negligible in comparison to the 15% and 10% requirements on steady-state error and percentage overshoot/undershoot respectively. Therefore, Control Case I and Case II can be assumed to be similar. It is also clearly evident from Table 3 that a prompt response is generated at a considerable cost of control energy. Despite expending such a large amount of control energy, the presence of steady-state error has not been eliminated.

In Section 3.4, the state feedback matrix  $K$  will be augmented with 4 SISO PI controllers. The feedback gain and SISO PI controllers will be simultaneously tuned with `looptune` to remove the steady-state error and keep the actuator torques below 100 Nm.

### 3.4 Structured $\mathcal{H}_\infty$ based `looptune`

The `looptune` command converts the user specified requirements of control bandwidth, rise time, settling time etc. into weighting functions. These functions are in turn translated into an  $\mathcal{H}_\infty$  optimization problem. `looptune` then invokes `system` to minimize the  $\mathcal{H}_\infty$  norm by tuning user specified parameters or objects in the control loop such as gains, transfer functions, state space models, etc.

To achieve the desired bandwidth, `looptune` tunes the parameters such that the open-loop gain crosses 0 dB in the crossover frequency interval specified by the user. Similarly, the open-loop response is shaped to perform integral action at low frequencies. Finally, the high-frequency roll-off exceeding -20 dB/decade guarantees robustness.

After successive trial and error, the gain crossover band is selected at  $0.1 \leq \omega \leq 100000$  rad/s. The control system response time and bandwidth are also determined in this particular region.

**3.4.1 State feedback gain augmented with SISO PI controllers (SFG-SISO PI).** To improve the transient and steady-state performance observed in Table 3, the feedback loop is modified to include scalar  $1 \times 1$  PI regulators. As depicted in Fig 6, a set of 4 SISO PI regulators is used, whereby each regulator is placed in series with each of the 4 actuators.

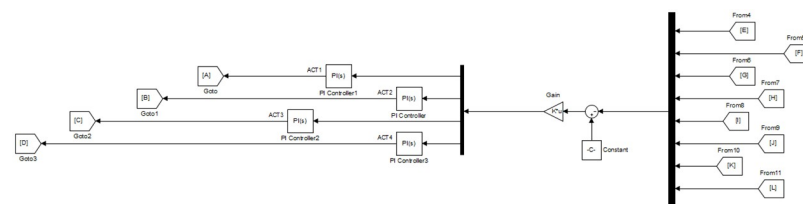


Fig 6. SFG-SISO PI control in Simulink.

<https://doi.org/10.1371/journal.pone.0266728.g006>

The `looptune` command is then applied to simultaneously find optimal values for the gains and  $\mathbf{K}$ . Eqs (11) and (12) represent the control law and closed loop error dynamics for the second control system respectively. The gains  $k_P$  and  $k_I$  respectively denote the proportional and integral gains. The proportional and integral gains are enclosed in  $4 \times 4$  matrices  $\mathbf{K}_{P-SISO}$  and  $\mathbf{K}_{I-SISO}$ , represented by (13) and (14) respectively.

$$\boldsymbol{\tau} = \mathbf{K}_{P-SISO} \mathbf{K} \tilde{\mathbf{x}}(t) + \mathbf{K}_{I-SISO} \mathbf{K} \int_{-\infty}^t \tilde{\mathbf{x}}(\alpha) d\alpha \tag{11}$$

$$\dot{\tilde{\mathbf{x}}} = (\mathbf{A} - \mathbf{B} \mathbf{K}_{P-SISO} \mathbf{K}) \tilde{\mathbf{x}}(t) - \mathbf{B} \mathbf{K}_{I-SISO} \mathbf{K} \int_{-\infty}^t \tilde{\mathbf{x}}(\alpha) d\alpha - \mathbf{A} \mathbf{r} \tag{12}$$

$$\mathbf{K}_{P-SISO} = \begin{bmatrix} k_{P1} & 0 & 0 & 0 \\ 0 & k_{P2} & 0 & 0 \\ 0 & 0 & k_{P3} & 0 \\ 0 & 0 & 0 & k_{P4} \end{bmatrix} \tag{13}$$

$$\mathbf{K}_{I-SISO} = \begin{bmatrix} k_{I1} & 0 & 0 & 0 \\ 0 & k_{I2} & 0 & 0 \\ 0 & 0 & k_{I3} & 0 \\ 0 & 0 & 0 & k_{I4} \end{bmatrix} \tag{14}$$

Since `looptune` requires an initial value for all of the tunable parameters present in the control loop,  $\mathbf{K}_{LQR}$  in (10) will be used to initialize `looptune` for tuning  $\mathbf{K}$ . The initial values for the proportional and integral gains are given by (15) and (16).

$$\mathbf{K}_{P-SISO-INIT.} = \begin{bmatrix} 1 & 0 & 0 & 0 \\ 0 & 1 & 0 & 0 \\ 0 & 0 & 1 & 0 \\ 0 & 0 & 0 & 1 \end{bmatrix} \tag{15}$$

$$\mathbf{K}_{I-SISO-INIT.} = \begin{bmatrix} 1 & 0 & 0 & 0 \\ 0 & 1 & 0 & 0 \\ 0 & 0 & 1 & 0 \\ 0 & 0 & 0 & 1 \end{bmatrix} \tag{16}$$

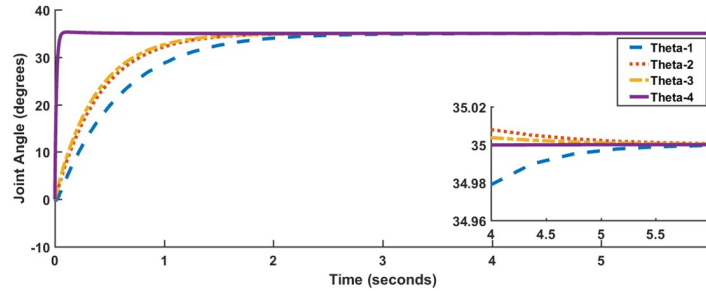


Fig 7. SFG-SISO PI response, Case I.

<https://doi.org/10.1371/journal.pone.0266728.g007>

At the end of the tuning process the final values for  $\mathbf{K}$ ,  $\mathbf{K}_{P-SISO}$  and  $\mathbf{K}_{I-SISO}$  are given as follows in (17), (18) and (19) respectively:

$$\mathbf{K}_{FINAL} = \begin{bmatrix} 0.0002 & -0.0015 & 0.0123 & 0.0698 & 2.8525 & -0.0000 & 1.5843 & 0.0004 \\ -0.0453 & 0.0215 & -0.0001 & 0.0068 & -0.0002 & 3.0005 & -0.0009 & 1.1751 \\ 3.0099 & 1.0951 & 0.0001 & -0.0061 & 0.0016 & -0.0399 & -0.0004 & 0.0160 \\ 0.0085 & -0.0173 & 2.8283 & 0.0423 & 0.0320 & 0.0007 & 0.0306 & -0.0002 \end{bmatrix} \quad (17)$$

$$\mathbf{K}_{P-SISO-FINAL} = \begin{bmatrix} 0.4695 & 0 & 0 & 0 \\ 0 & 0.6536 & 0 & 0 \\ 0 & 0 & 0.6597 & 0 \\ 0 & 0 & 0 & 0.2564 \end{bmatrix} \quad (18)$$

$$\mathbf{K}_{I-SISO-FINAL} = \begin{bmatrix} 0.9991 & 0 & 0 & 0 \\ 0 & 0.9999 & 0 & 0 \\ 0 & 0 & 1.0000 & 0 \\ 0 & 0 & 0 & 1.0000 \end{bmatrix} \quad (19)$$

Joint angle responses are shown in Fig 7, while Fig 8 shows actuator torques. Since the response and actuator torque profiles of Case I and Case II are similar, only the plots of Case I have been shown. It is evident from both Figs 7 and 8 that not only has the steady-state error been removed but also less control effort is expended. The degradation in transient parameters

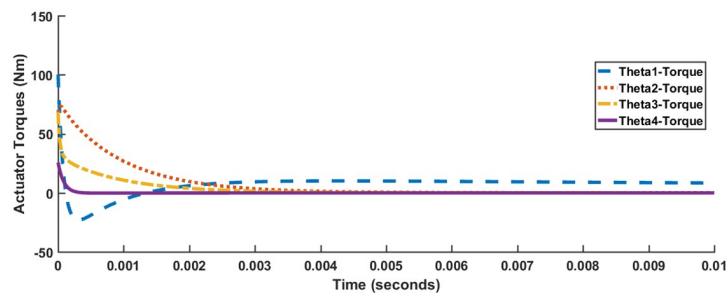


Fig 8. SFG-SISO PI actuator response, Case I.

<https://doi.org/10.1371/journal.pone.0266728.g008>

**Table 4. Summary of results for SFG-SISO PI controllers.**

Case	$\theta_I$	$\theta_F$	Overshoot (%)	Undershoot (%)	Settling Time (s)	Rise Time (s)	Peak Absolute Torque (Nm)	Steady-State Error (%)
I	0	35	0	0.5316	2.1867	1.2366	100.2736	0
	0	35	0.04469	0.007096	1.5051	0.8727	73.2847	0
	0	35	0.01779	0	1.4364	0.8143	68.6127	0
	0	35	0.7894	0	0.05053	0.03026	25.7508	0
II	35	70	0	0	2.1734	1.2111	100.2736	0
	35	70	0.01510	0	1.4748	0.8522	68.2612	0
	35	70	0.0003536	0	1.441	0.8122	68.6127	0
	35	70	0.3873	0	0.05069	0.03029	25.7508	0

<https://doi.org/10.1371/journal.pone.0266728.t004>

such as rise time and settling appears to be negligible for angles,  $\theta_2$  and  $\theta_3$  while there is considerable improvement in the response of  $\theta_4$ . Table 4 summarizes the results for SFG-SISO PI.

Similar to Table 3, the values of Case I and Case II in Table 4 are similar in terms of settling time, rise time, peak absolute torque, and steady-state error, with a maximum variation of 7% in peak absolute torque for joint angle  $\theta_2$ . Again, the difference in values of overshoot and undershoot are insignificant when compared with the requirement of 15%.

**3.4.2 State feedback gain augmented with MIMO integral gain (SFG-MIMO PI).** For the third control system, a single  $4 \times 8$  matrix  $K_I$  is added in the feedback loop and cascaded with an integrator. The output from the integrator block is summed with the output from the state feedback matrix  $K_P$ .

The main difference from the second control system lies in the fact that both  $K_I$  and  $K_P$  are  $4 \times 8$  matrix gains as opposed to  $1 \times 1$  scalar  $k_p$  and  $k_i$  gains. The gain  $K_P$  is simultaneously acting as a state feedback gain as well as proportional gain in the third control system. On the other hand, the state feedback gain  $K$  in SFG-SISO PI is separate from the proportional gain  $k_p$ . The implementation of this scheme is shown in Fig 9.

Here  $K_P$  is obtained by tuning  $K_{IQR}$  computed in (10). This results in a MIMO PI controller. Eqs (20) and (21) describe the dynamics of this controller.

$$\tau = K_P \tilde{x}(t) + K_I \int_{-\infty}^t \tilde{x}(\alpha) d\alpha \tag{20}$$

$$\dot{\tilde{x}} = (A - BK_P) \tilde{x}(t) - BK_I \int_{-\infty}^t \tilde{x}(\alpha) d\alpha - Ar \tag{21}$$

The integral gain  $K_I$  will be initialized by the value given in (22). The final tuned values of  $K_P$  and  $K_I$  are shown in (23) and (24) respectively. Figs 6 and 7 show the response for joint

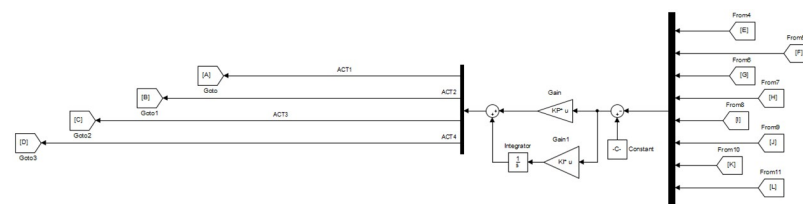


**Fig 9. SFG-MIMO PI control in Simulink.**

<https://doi.org/10.1371/journal.pone.0266728.g009>

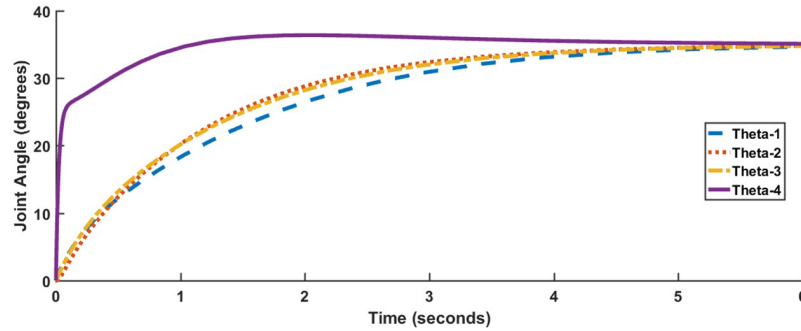


Fig 10. SFG-MIMO PI response, Case I.

<https://doi.org/10.1371/journal.pone.0266728.g010>

angles and the actuator torques for Case I respectively.

$$K_{I-INITIAL} = \begin{bmatrix} 2 & 2 & 2 & 2 & 2 & 2 & 2 & 2 \\ 2 & 2 & 2 & 2 & 2 & 2 & 2 & 2 \\ 2 & 2 & 2 & 2 & 2 & 2 & 2 & 2 \\ 2 & 2 & 2 & 2 & 2 & 2 & 2 & 2 \end{bmatrix} \quad (22)$$

$$K_{P-FINAL} = \begin{bmatrix} -0.0387 & -0.1626 & -0.2321 & 0.0152 & 2.7122 & -0.0327 & 1.2367 & -0.1113 \\ -0.0429 & -0.0034 & -0.0751 & 0.0917 & -0.1372 & 3.0417 & 0.0582 & 1.2559 \\ 3.0082 & 1.2135 & -0.0831 & 0.0397 & -0.1162 & -0.0205 & -0.0010 & -0.0671 \\ 0.0163 & 0.0076 & 2.8202 & 0.0882 & 0.0046 & 0.0947 & -0.0095 & -0.0130 \end{bmatrix} \quad (23)$$

$$K_{I-FINAL} = \begin{bmatrix} 1.1252 & 2.0603 & 1.1471 & 1.8759 & 4.3302 & 1.1130 & 2.4178 & 2.0772 \\ 1.1307 & 2.0609 & 1.1362 & 1.9844 & 1.1922 & 4.4679 & 1.9819 & 2.1491 \\ 4.4781 & 2.1191 & 1.1280 & 2.0377 & 1.1739 & 1.1227 & 1.9686 & 2.0709 \\ 1.5491 & 1.5771 & 4.7664 & 1.3251 & 1.5324 & 1.5733 & 1.4617 & 1.5500 \end{bmatrix} \quad (24)$$

It is evident from Figs 10 and 11 that in comparison to both LQR and SFG-SISO PI, the SFG-MIMO PI controller is slow. Except for angle  $\theta_1$ , actuator effort for SFG-MIMO PI is

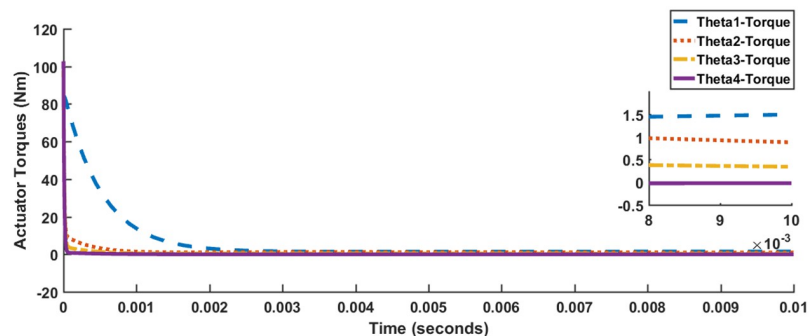


Fig 11. SFG-MIMO PI actuator response, Case I.

<https://doi.org/10.1371/journal.pone.0266728.g011>

Table 5. Summary of results for SFG-MIMO PI.

Case	$\theta_I$	$\theta_F$	Overshoot (%)	Undershoot (%)	Settling Time (s)	Rise Time (s)	Peak Absolute Torque (Nm)	Steady-State Error (%)
I	0	35	0.001490	0.001416	5.1059	3.112089	84.3345	0.0002190
	0	35	0.0003520	0.08442	4.5631	2.51783	97.5285	0.00005200
	0	35	0.0003090	0	4.6920	2.712955	97.5978	0.00005370
	0	35	3.9675	0	3.6240	0.577677	102.7510	0.00003490
II	35	70	0.0001860	0	5.1547	3.0930	84.3043	0
	35	70	0.0002980	0	4.6126	2.5325	97.5285	0
	35	70	0.00008620	0	4.7081	2.7163	97.5978	0
	35	70	1.9562	0	3.6394	0.5902	102.7510	0

<https://doi.org/10.1371/journal.pone.0266728.t005>

greater than SFG-SISO PI. However, actuator effort for SFG-MIMO PI is still less than LQR for all joint angles. Numerical results for SFG-MIMO PI are presented in Table 5.

As discussed previously, the values of Case I and Case II are similar in terms of settling time, rise time and peak absolute torque, with maximum variation being 2%. When considering the requirement of Table 2, the differences in overshoot and undershoot are negligible for all the joint angles except for  $\theta_4$ . The values of overshoot observed for joint angle  $\theta_4$ , although different is nonetheless comparable.

## 5 Trajectory tracking control

Robotic manipulators perform pick and place tasks as one of their primary functions. In such cases, the manipulator has to follow a predefined time dependent trajectory as shown in Fig 12. Figs 13 and 14 show the trajectory tracking error for SFG-SISO PI and SFG-MIMO PI schemes respectively. The tracking error shown is the numerical difference between the input reference and the actual output response.

For both controllers, a finite steady-state error is observed during the rise and fall parts of the trajectory, which is within the  $\pm 10\%$  limit given in Table 2. The steady-state error converges to zero as soon as the trajectory attains a constant value. This result is consistent with the expected behavior of a Type I control system. It is evident from both Figs 13 and 14 that SFG-SISO PI control has a comparatively smaller tracking error for all of the joint angles. In both cases, however, tracking error is the largest for the angle  $\theta_1$ , followed jointly by the angles  $\theta_2$  and  $\theta_3$ . Remarkably,  $\theta_4$  shows minimum tracking error.

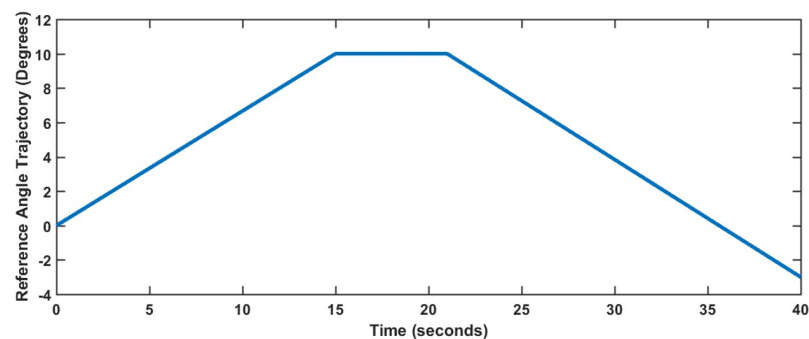
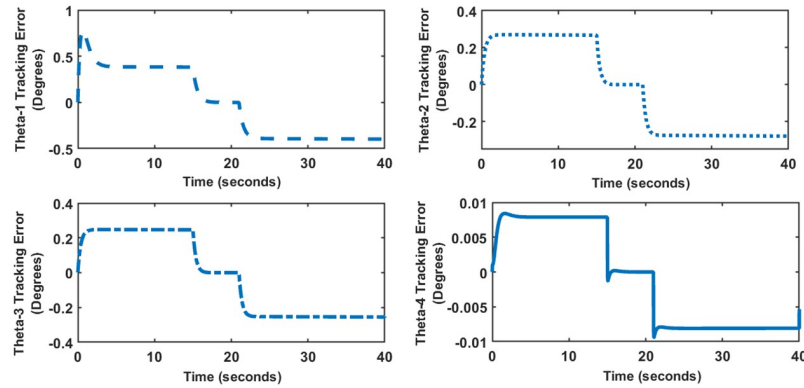


Fig 12. Reference trajectory for the robotic manipulator.

<https://doi.org/10.1371/journal.pone.0266728.g012>



**Fig 13. Tracking error for SFG-SISO PI control.**

<https://doi.org/10.1371/journal.pone.0266728.g013>

### 4 Analysis of results

The results for the three control schemes are now compared in Table 6. The results are compared in terms of percentage reduction achieved with respect to the performance benchmarks specified in Table 2. Only the results for Case I are discussed since the results of Case II are more or less similar in terms of settling time, rise time and peak absolute torque for all three of the controllers as discussed above.

It is apparent from Table 6 that there is a certain tradeoff involved between improvement in performance and controller effort. For example, the peak torque reduction for joint angle  $\theta_1$  in SFG-SISO PI control is only 9% more than the peak torque reduction for LQR. Correspondingly, the reduction in the rise time and settling times is 15% and 13% lower in SFG-SISO PI as compared to LQR control. Remarkably, the reduction in peak actuator torque of by 44% and 47% in SFG-SISO PI for joint angles  $\theta_2$  and  $\theta_3$ , gives nearly the same reduction in settling time and rise time as LQR control. For angle  $\theta_4$  however, an 80% reduction in peak absolute torque brings about 99% reduction in rise time and settling time, which is truly remarkable.

For SFG-MIMO PI control, the peak torque reduction  $\theta_1$  is 21% greater when compared to LQR. However, the reduction in rise and settling times is 70% and 62% less respectively. Similarly, for joint angle  $\theta_2$  a reduction of 16% and 24% is respectively observed in rise time and settling time for a 25% decrease in actuator torque. Results of the joint angle  $\theta_3$  are more or less similar to the angle  $\theta_2$ . In  $\theta_4$ , the rise time reduction is 4% greater than the corresponding

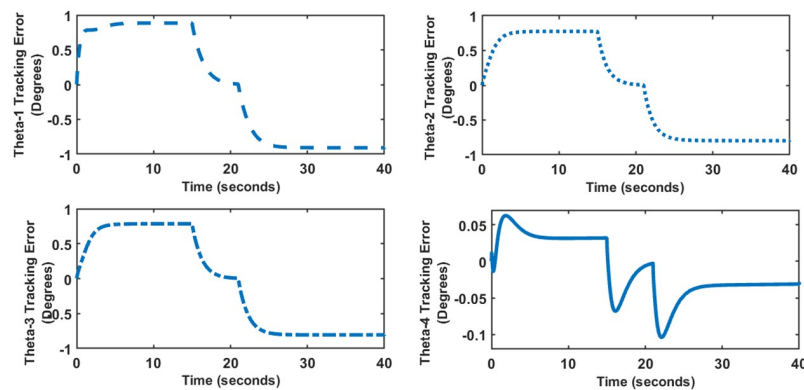


**Fig 14. Tracking error for SFG-MIMO PI control.**

<https://doi.org/10.1371/journal.pone.0266728.g014>

Table 6. Comparison of results in terms of percentage reduction.

Angle	Control Scheme	Overshoot Reduction %	Undershoot Reduction %	Settling Time Reduction %	Rise Time Reduction %	Peak Absolute Torque Reduction %	Steady-State Error Reduction %
$\theta_1$	LQR	100	100	77	74	14	90
	SFG-SISO PI	100	96	64	59	23	100
	SFG-MIMO PI	100	100	15	4	35	100
$\theta_2$	LQR	100	100	76	73	5	92
	SFG-SISO PI	100	100	75	71	44	100
	SFG-MIMO PI	100	99	24	16	25	100
$\theta_3$	LQR	100	100	78	75	15	96
	SFG-SISO PI	100	100	76	73	47	100
	SFG-MIMO PI	100	100	22	10	25	100
$\theta_4$	LQR	100	100	79	77	15	100
	SFG-SISO PI	95	100	99	99	80	100
	SFG-MIMO PI	74	100	40	81	21	100

<https://doi.org/10.1371/journal.pone.0266728.t006>

value in LQR control but the settling time reduction is 39% less for a 21% reduction in actuator torque. In light of the above results, the SFG-SISO PI control is a better option compared to both LQR and SFG-MIMO PI in terms of tradeoff or balance between controller effort and performance.

## 5 Uncertainty analysis

Since no mathematical model of any physical system can be fully accurate, there will always be an element of uncertainty in any control system design. One of the ways in which the effect of uncertainty in robotic manipulators can be observed is to affect parametric changes in the manipulator system. This is done by increasing the mass of all individual links simultaneously by 3, 5, 7 and 9 times and observing the transient and steady-state performance.

Only the results of the joint angle  $\theta_1$  (Case I) have been shown since the plots of other joint angles are more or less the same. Figs 15–17 show the results for LQR, SFG-SISO PI and SFG-MIMO PI under mass variation respectively. It can be observed from Fig 15 that the steady-error increases in proportion to the increase in mass. Thus, it can be concluded that LQR control lacks robustness. Figs 16 and 17 on the other hand do not show appreciable

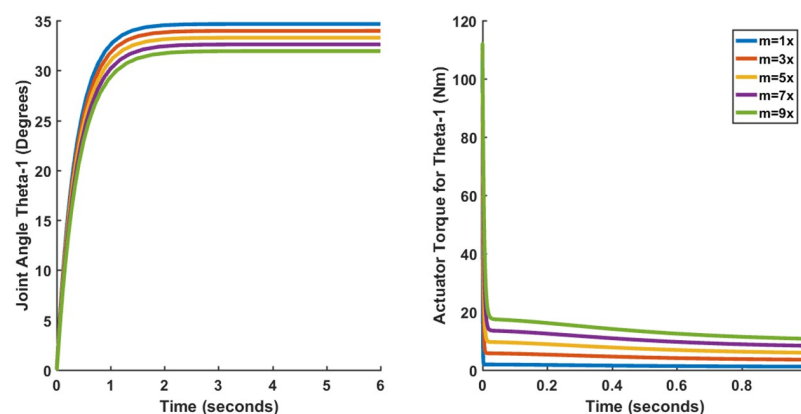
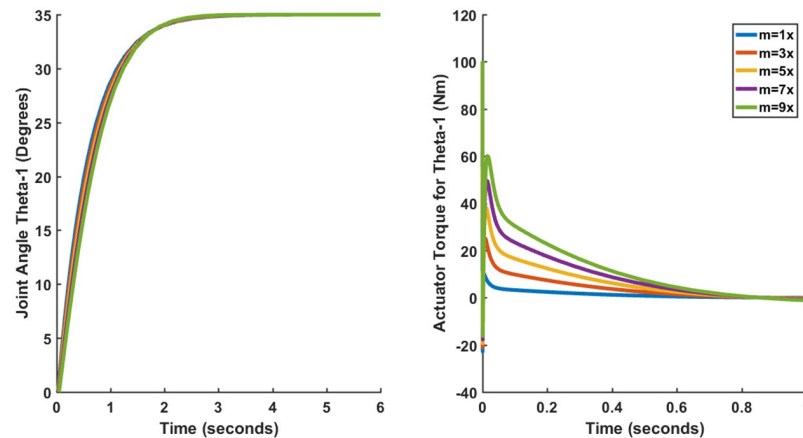


Fig 15. Performance of LQR (Case I) under mass variation.

<https://doi.org/10.1371/journal.pone.0266728.g015>



**Fig 16. Performance of SFG-SISO (Case I) under mass variation.**

<https://doi.org/10.1371/journal.pone.0266728.g016>

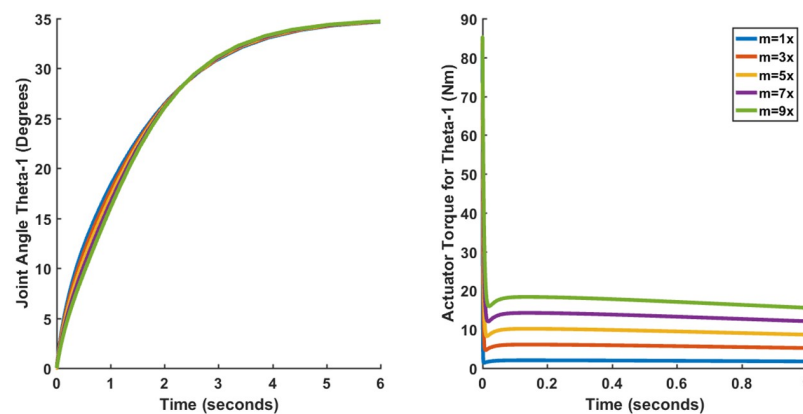


**Fig 17. Performance of SFG-MIMO (Case I) under mass variation.**

<https://doi.org/10.1371/journal.pone.0266728.g017>

deviation from the results presented earlier in Section 3.4. Therefore, both SFG-SISO PI and SFG-MIMO PI controllers show robustness to uncertainty. The only difference discernable is that the actuator torque takes a longer time to converge as the mass of each link increases. Nevertheless, there is little or no difference in peak actuator torque.

## 6 Conclusion

LQR and `looptune` were compared in terms of transient and steady-state performance, and robustness to uncertainty using a 4-DOF robotic arm. For this purpose, three different full state feedback control architectures were developed. The feedback gain for the first control system was computed using LQR. In comparison, SFG-SISO PI and SFG-MIMO PI controllers were synthesized by `looptune`. The SFG-SISO PI and SFG-MIMO PI controllers were also compared in terms of trajectory tracking. The value of the state feedback gain calculated using LQR was used as an initial value by `looptune`. Despite expending a large amount of control effort, the LQR was unable to eliminate steady-state error. Moreover, it was found to lack robustness against increasing mass variation. The SFG-SISO PI controller delivered a slightly slow response by considerably reducing its control effort. It also eliminated the steady-state error while showing robustness to uncertainty. For a slight decrease in control effort, the

response of SFG-MIMO PI controller was slowest. However, it still showed robustness to uncertainty. Therefore, from an overall perspective, the SFG-SISO PI controller fares as the best controller, validates the superiority of `looptune` over LQR and affirms the potential of `looptune` for future control system applications.

In this research, we have proposed a Type-I (position control) system for a rigid robotic arm. The proposed methodology may be extended to include velocity or acceleration control. This can prove highly useful in the context of robotic automation processes such as welding, painting, packaging, pick and drop etc. In addition, it has been assumed that all of the states are measurable. Practically, one or more of the states may not be measurable, necessitating the requirement of an observer. Consequently, the performance of a Linear Quadratic Gaussian (LQG) (or other observer based controllers) may be compared against `looptune` synthesized observer based controllers. Likewise, `looptune` synthesized controllers can also be compared against adaptive or intelligent controllers discussed in Section 1. The performance or robustness of `looptune` can also be compared against manually tuned  $\mathcal{H}_2$  and  $\mathcal{H}_\infty$  controllers. Finally, the performance of `looptune` can be evaluated for flexible robotic manipulator models. In summary, there are multiple directions in which the methodology applied in this paper can be explored or further improved.

## Author Contributions

**Conceptualization:** Arafat Asghar, Muhammad Iqbal.

**Formal analysis:** Arafat Asghar.

**Investigation:** Arafat Asghar.

**Methodology:** Arafat Asghar, Jamshed Iqbal.

**Project administration:** Arafat Asghar.

**Resources:** Abdul Khaliq.

**Software:** Saif ur Rehman.

**Supervision:** Muhammad Iqbal, Abdul Khaliq, Jamshed Iqbal.

**Validation:** Arafat Asghar, Jamshed Iqbal.

**Writing – original draft:** Arafat Asghar, Saif ur Rehman.

**Writing – review & editing:** Abdul Khaliq, Jamshed Iqbal.

## References

1. Iqbal J, Al-Zahrani A, Alharbi SA, Hashmi A. Robotics inspired renewable energy developments: prospective opportunities and challenges. *IEEE Access*. 2019; 7: 174898–923. <https://doi.org/10.1109/ACCESS.2019.2957013>
2. He W, Li Z, Chen CLP. A survey of human-centered intelligent robots: issues and challenges. *IEEE/CAA Journal of Automatica Sinica*. 2017; 4(4): 602–9. <https://doi.org/10.1109/JAS.2017.7510604>
3. Ilyas M, Iqbal J, Ahmad S, Uppal AA, Imtiaz WA, Riaz RA. Hypnosis regulation in propofol anaesthesia employing super-twisting sliding mode control to compensate variability dynamics. *IET Systems Biology*. 2020; 14(2): 59–67. <https://doi.org/10.1049/iet-syb.2018.5080> PMID: 32196464
4. Ilyas M, Khaqan A, Iqbal J, Riaz RA. Regulation of hypnosis in Propofol anesthesia administration based on non-linear control strategy. *Brazilian Journal of Anesthesiology (English Edition)*. 2017 Mar 1; 67(2): 122–30. <https://doi.org/10.1016/j.bjane.2015.08.011>
5. Zhang Q, Wang H. A novel data-based stochastic distribution control for non-Gaussian stochastic systems. *IEEE Transactions on Automatic Control*. 2022 Mar; 67(3): 1506–13.

6. Jin M, Kang SH, Chang PH, Lee J Robust control of robot manipulators using inclusive and enhanced time delay control. *IEEE/ASME Transactions on Mechatronics*. 2017 Oct; 22(5): 2141–52. <https://doi.org/10.1109/TMECH.2017.2718108>
7. Iqbal J. Modern control laws for an articulated robotic arm: modeling and simulation. *Engineering, Technology and Applied Science Research*. 2019 Apr 10; 9(2): 4057–61. <https://doi.org/10.48084/etasr.2598>
8. Mattila J, Koivumäki J, Caldwell DG, Semini C. A survey on control of hydraulic robotic manipulators with projection to future trends. *IEEE/ASME Transactions on Mechatronics*. 2017 Apr; 22(2): 669–80. <https://doi.org/10.1109/TMECH.2017.2668604>
9. Sayahkarajy M, Mohamed Z, Mohd Faudzi AA. Review of modelling and control of flexible-link manipulators. *Proceedings of the Institution of Mechanical Engineers, Part I: Journal of Systems and Control Engineering*. 2016 Sep 1; 230(8): 861–73.
10. Liu Y, Zhang Q, Yue H. Stochastic distribution tracking control for stochastic non-linear systems via probability density function vectorisation. *Transactions of the Institute of Measurement and Control*. 2021 Oct 1; 43(14): 3149–57. <https://doi.org/10.1177/01423312211016929>
11. Wang H. Adaptive control of robot manipulators with uncertain kinematics and dynamics. *IEEE Transactions on Automatic Control*. 2017 Feb; 62(2): 948–54. <https://doi.org/10.1109/TAC.2016.2575827>
12. Zhang D, Wei B. A review on model reference adaptive control of robotic manipulators. *Annual Reviews in Control*. 2017 Jan 1; 43: 188–98. <https://doi.org/10.1016/j.arcontrol.2017.02.002>
13. Zhang D, Wei B. Critical review and progress of adaptive controller design for robot arms. *Mechatronics and Robotics Engineering for Advanced and Intelligent Manufacturing*. 2017: 3–12. [https://doi.org/10.1007/978-3-319-33581-0\\_1](https://doi.org/10.1007/978-3-319-33581-0_1)
14. Khan O, Pervaiz M, Ahmad E, Iqbal J. On the derivation of novel model and sophisticated control of flexible joint manipulator. *Revue Roumaine des Sciences Techniques—Serie Électrotechnique et Énergétique*. 2017 Apr 1; 62:103–8.
15. Iqbal J, Ullah MI, Khan AA, Irfan M. Towards sophisticated control of robotic manipulators: an experimental study on a pseudo-industrial arm. *Strojniski Vestnik—Journal of Mechanical Engineering*. 2015 Jul 1; 61(7–8): 465–72. <https://doi.org/10.5545/sv-jme.2015.2511>
16. Awan ZS, Ali K, Iqbal J, Mehmood A. Adaptive backstepping based sensor and actuator fault tolerant control of a manipulator. *Journal of Electrical Engineering and Technology*. 2019 Oct 11; 14. <https://doi.org/10.1007/s42835-019-00277-9>
17. Izadbakhsh A. Robust adaptive control of voltage saturated flexible joint robots with experimental evaluations. *AUT Journal of Modeling and Simulation*. 2018 Jun 1; 50(1):31–8.
18. Anderson B, Dehghani A. Challenges of adaptive control—past, permanent and future. *Annual reviews in control*. 2008 Dec 1; 32(2): 123–35. <https://doi.org/10.1016/j.arcontrol.2008.06.001>
19. Dehghani A, Anderson BDO, Lanzon A. Unfalsified adaptive control: A new controller implementation and some remarks. In: 2007 European Control Conference (ECC). 2007. p. 709–16.
20. Stefanovic M, Safonov MG. *Safe adaptive control: Data-driven stability analysis and robust synthesis*. Springer; 2011 Feb 4.
21. Wang R, Paul A, Stefanovic M, Safonov MG. Cost detectability and stability of adaptive control systems. *International Journal of Robust and Nonlinear Control: IFAC Affiliated Journal*. 2007 Mar 25; 17(5-6): 549–61. <https://doi.org/10.1002/mc.1122>
22. Sheng N, Zhang D, Zhang Q. Fuzzy command filtered backstepping control for nonlinear system with nonlinear faults. *IEEE Access*. 2021; 9: 60409–18. <https://doi.org/10.1109/ACCESS.2021.3074424>
23. Cai ZX. *Intelligent control: principles, techniques and applications*. World Scientific; 1997. p. 10–11.
24. Vassilyev SN, Kelina AY, Kudinov YI, Pashchenko FF. *Intelligent control systems*. Procedia Computer Science. 2017 Jan 1; 103: 623–8.
25. Yu X, He W, Li H, Sun J. Adaptive fuzzy full-state and output-feedback control for uncertain robots with output constraint. *IEEE Transactions on Systems, Man, and Cybernetics: Systems*. 2021 Nov; 51(11): 6994–7007. <https://doi.org/10.1109/TSMC.2019.2963072>
26. Yu X, He W, Li Q, Li Y, Li B. Human-robot co-carrying using visual and force sensing. *IEEE Transactions on Industrial Electronics*. 2021 Sep; 68(9): 8657–66. <https://doi.org/10.1109/TIE.2020.3016271> PMID: 34398646
27. Zhang X, Qiao S, Quan L, Ge L. Velocity and position hybrid control for excavator boom based on independent metering system *IEEE Access*. 2019; 7: 71999–2011.
28. Chen X, Yu Z, Zhang W, Zheng Y, Huang Q, Ming A. Bioinspired control of walking with toe-off, heel-strike, and disturbance rejection for a biped robot *IEEE Transactions on Industrial Electronics*. 2017 Oct; 64(10): 7962–71. <https://doi.org/10.1109/TIE.2017.2698361>

29. Ajwad SA, Iqbal J, Islam RU, Alsheikhy A, Almeshal A, Mehmood A. Optimal and robust control of multi DOF robotic manipulator: design and hardware realization. *IEEE Transactions on Cybernetics*. 2017 Feb; 47(2): 365–77.
30. Ajwad SA, Iqbal J, Khan AA, Mehmood A. Disturbance-observer-based robust control of a serial-link robotic manipulator using SMC and PBC techniques. *Studies in Informatics and Control*. 2015 Dec 1; 24(4): 401–8. <https://doi.org/10.24846/v24i4y201504>
31. Alam W, Mehmood A, Ali K, Javaid U, Alharbi S, Iqbal J. Nonlinear control of a flexible joint robotic manipulator with experimental validation. *Strojniški vestnik-Journal of Mechanical Engineering*. 2018 Jan 17; 64(1): 47–55.
32. Ullah MI, Ajwad SA, Irfan M, Iqbal J. Non-linear control law for articulated serial manipulators: simulation augmented with hardware implementation. *Elektronika ir Elektrotechnika*. 2016 Feb 4; 22(1): 3–7. <https://doi.org/10.5755/j01.eee.22.1.14094>
33. Iqbal J, Ullah M, Khan SG, Khelifa B, Ćuković S. Nonlinear control systems—a brief overview of historical and recent advances. *Nonlinear Engineering*. 2017 Dec 1; 6(4): 301–12. <https://doi.org/10.1515/nleng-2016-0077>
34. Ajwad SA, Iqbal J, Ullah MI, Mehmood A. A systematic review of current and emergent manipulator control approaches. *Frontiers of mechanical engineering*. 2015 Jun; 10(2): 198–210. <https://doi.org/10.1007/s11465-015-0335-0>
35. Ajwad S, Ullah M, Baizid K, Iqbal J. A comprehensive state-of-the-art on control of industrial articulated robots. *Journal of the Balkan Tribological Association*. 2014 Jan 1; 20: 499–521.
36. Raffo GV, Ortega MG, Rubio FR. MPC with nonlinear  $H_\infty$  control for path tracking of a quad-rotor helicopter. *IFAC Proceedings Volumes*. 2008 Jan 1; 41(2): 8564–9. <https://doi.org/10.3182/20080706-5-KR-1001.01448>
37. Ullah S, Mehmood A, Khan Q, Rehman S, Iqbal J. Robust integral sliding mode control design for stability enhancement of under-actuated quadcopter. *International Journal of Control, Automation and Systems*. 2020 Jul; 18(7): 1671–8. <https://doi.org/10.1007/s12555-019-0302-3>
38. Iqbal S, Bhatti AI. Load varying polytopic based robust controller design in LMI framework for a 2-DOF stabilized platform. *Arabian Journal for Science and Engineering*. 2011 Mar; 36(2): 311–27. <https://doi.org/10.1007/s13369-010-0022-8>
39. Chavez Guzmán CA, Aguilar Bustos LT, Mérida Rubio JO. Analysis and synthesis of global nonlinear controller for robot manipulators. *Mathematical Problems in Engineering*. 2015 Apr 5; 2015. <https://doi.org/10.1155/2015/410873>
40. Liu H, Tian X, Wang G, Zhang T. Finite-time  $H_\infty$  control for high-precision tracking in robotic manipulators using backstepping control. *IEEE Transactions on Industrial Electronics*. 2016 Sep; 63(9): 5501–13. <https://doi.org/10.1109/TIE.2016.2583998>
41. Luo Y, Wang Z, Liang J, Wei G, Alsaadi FE.  $H_\infty$  control for 2-D fuzzy systems with interval time-varying delays and missing measurements. *IEEE Transactions on Cybernetics*. 2017 Feb; 47(2): 365–77. PMID: 26887020
42. Luo Y, Wang Z, Wei G, Alsaadi FE. Nonfragile  $l_2$ - $l_\infty$  fault estimation for markovian jump 2-D systems with specified power bounds *IEEE Transactions on Systems, Man, and Cybernetics: Systems*. 2020 May; 50(5): 1964–75. <https://doi.org/10.1109/TSMC.2018.2794414>
43. Rigatos G, Siano P, Raffo G.N. An H-infinity nonlinear control approach for multi-DOF robotic manipulators. *IFAC-PapersOnLine*. 2016 Jan 1; 49(12): 1406–11. <https://doi.org/10.1016/j.ifacol.2016.07.766>
44. He W, Dong Y. Adaptive fuzzy neural network control for a constrained robot using impedance learning. *IEEE Transactions on Neural Networks and Learning Systems*. 2018 Apr; 29(4): 1174–86. <https://doi.org/10.1109/TNNLS.2017.2665581> PMID: 28362618
45. Lashin M, Fanni M, Mohamed AM, Miyashita T. Dynamic modeling and inverse optimal PID with feed-forward control in  $H_\infty$  framework for a novel 3D pantograph manipulator. *International Journal of Control, Automation and Systems*. 2018 Feb; 16(1): 39–54. <https://doi.org/10.1007/s12555-016-0740-0>
46. Azar AT, Serrano FE, Hameed IA, Kamal NA, Vaidyanathan S. Robust h-infinity decentralized control for industrial cooperative robots. In *International Conference on Advanced Intelligent Systems and Informatics*. 2019 Oct; p. 254–265.
47. Gahinet P, Apkarian P. A linear matrix inequality approach to  $H_\infty$  control. *International Journal of Robust and Nonlinear Control*. 1994; 4(4): 421–48. <https://doi.org/10.1002/rnc.4590040403>
48. Doyle JC, Glover K, Khargonekar PP, Francis BA. State-space solutions to standard  $H_2$  and  $H_\infty$  control problems. *IEEE Transactions on Automatic Control*. 1989 Aug; 34(8): 831–47. <https://doi.org/10.1109/9.29425>
49. Apkarian P, Noll D. Nonsmooth  $H_\infty$  synthesis *IEEE Transactions on Automatic Control*. 2006 Jan; 51(1): 71–86. <https://doi.org/10.1109/TAC.2005.860290>

50. Bruinsma NA, Steinbuch M. A fast algorithm to compute the  $H_\infty$ -norm of a transfer function matrix. *Systems and Control Letters*. 1990 Apr 1; 14(4): 287–93. [https://doi.org/10.1016/0167-6911\(90\)90049-Z](https://doi.org/10.1016/0167-6911(90)90049-Z)
51. Gahinet P, Apkarian P. Decentralized and fixed-structure  $H_\infty$  control in MATLAB. In: 2011 50th IEEE conference on decision and control and european control conference. 2011 Dec; p. 8205–8210.
52. Gahinet P, Apkarian P. Structured  $H_\infty$  synthesis in MATLAB. *IFAC Proceedings Volumes*. 2011 Jan 1; 44(1): 1435–40. <https://doi.org/10.3182/20110828-6-IT-1002.00708>
53. Gahinet P, Apkarian P. Frequency-domain tuning of fixed-structure control systems. In: *Proceedings of 2012 UKACC International Conference on Control*. 2012; p. 178–83
54. Abroug N, Laroche E. Structured  $H_\infty$  framework for impedance minimization on robot arm with compliant actuation. In: *2014 IEEE Conference on Control Applications (CCA)*. 2014. p. 1300–5.
55. Halalchi H, Laroche E, Bara GI. Flexible-link robot control using a linear parameter varying systems methodology. *International Journal of Advanced Robotic Systems*. 2014 Mar 1; 11(3): 46. <https://doi.org/10.5772/57325>
56. Dubanchet V, Saussié D, Alazard D, Bérard C, Peuvédic CL. Motion planning and control of a space robot to capture a tumbling debris. In: *Advances in Aerospace Guidance, Navigation and Control*. Cham: Springer International Publishing; 2015. p. 699–717.
57. Dubanchet V, Saussié D, Alazard D, Bérard C, Peuvédic CL. Modeling and control of a space robot for active debris removal. *CEAS Space Journal*. 2015 Jun 1; 7(2): 203–18. <https://doi.org/10.1007/s12567-015-0082-4>
58. Chabir A, Boukhnifer M, Bouteraa Y, Chaibet A, Ghommam J. Modelling and fixed order robust  $H_\infty$  control of aerial vehicle: Simulation and experimental results. *COMPEL: International Journal for Computation and Mathematics in Electrical and Electronic engineering*. 2016; 35(3): 1064–85. <https://doi.org/10.1108/COMPEL-06-2015-0217>
59. Marcos A, Sato M. Flight testing of an structured H-infinity controller: An EU-Japan collaborative experience. In: *2017 IEEE Conference on Control Technology and Applications (CCTA)*. 2017; p. 2132–7.
60. Trung TV, Iwasaki M.  $H_\infty$  control-based vibration suppression in robot arm with strain wave gearing. In: *2018 International Power Electronics Conference (IPEC-Niigata 2018—ECCE Asia)*. 2018; p. 1666–72.
61. Costacurta J, Osborn L, Thakor N, Sarma S. Designing feedback controllers for human-prosthetic systems using  $H_\infty$  model matching. In: *2018 40th Annual International Conference of the IEEE Engineering in Medicine and Biology Society (EMBC)*. 2018 Jul 18; p. 2316–2319.
62. Wang X, Xiang C, Xu B, Fan W. System identification and robust stabilization using structured controller for a novel ducted fan flying robot. *Proceedings of the Institution of Mechanical Engineers, Part G: Journal of Aerospace Engineering*. 2019 Jan 1; 233(1): 197–214. <https://doi.org/10.1177/0954410017728970>
63. Trung T, Iwasaki M. Robust 2-DOF controller design using  $H_\infty$  synthesis for flexible robots. *IEEJ Journal of Industry Applications*. 2019 Jul 1; 8: 623–31. <https://doi.org/10.1541/ieejia.8.623>
64. Ajwad S, Mehmood A, Ullah M, Iqbal J. Optimal v/s robust control: A study and comparison for articulated manipulator. *Journal of the Balkan Tribological Association*. 2016 Oct 17; 22: 2460–6.
65. Islam R, Iqbal J, Khan Q. Design and comparison of two control strategies for multi-DOF articulated robotic arm manipulator. *Journal of Control Engineering and Applied Informatics*. 2014 Jun 25; 16(2): 28–39.
66. Shakibjoo AD, Shakibjoo MD. 2-DOF PID with reset controller for 4-DOF robot arm manipulator. In: *2015 International Conference on Advanced Robotics and Intelligent Systems (ARIS)*. 2015; p. 1–6.
67. Wang X, Xiang C, Xu B, Najjaran H. Robust and adaptive control of a novel ducted fan vehicle in the presence of actuator uncertainties and saturation. In: *2017 International Conference on Unmanned Aircraft Systems (ICUAS)*. 2017; p. 1516–21.
68. Zhao D, Winward E, Yang Z, Stobart R, Steffen T. Robust control of electrified turbocharged diesel engines. In: *2016 IEEE 55th Conference on Decision and Control (CDC)*. 2016; p. 734–9.
69. González PJ, Guimarães Neto AB, Barbosa GC, Bertolin RM, Silvestre FJ, Cesnik CE. X-hale autopilot with stability augmentation and shape control based on loop separation. In: *Proceedings of the International Forum on Aeroelasticity and Structural Dynamics (IFASD)*. 2017 Jun;
70. Wasim M, Ullah M, Iqbal J. Gain-scheduled proportional integral derivative control of taxi model of unmanned aerial vehicles. *Revue Roumaine des Sciences Techniques—Serie Électrotechnique et Énergétique*. 2019 Mar 31; 64: 75–80.
71. Samad T. A survey on industry impact and challenges thereof. *IEEE Control Systems Magazine*. 2017 Feb; 37(1): 17–8. <https://doi.org/10.1109/MCS.2016.2621438>
72. Nise N. Steady-state errors. In: *Control Systems Engineering*. 7th ed. NJ, USA: Hoboken; p. 345–8.

73. Al-Qahtani HM, Mohammed AA, Sunar M. Dynamics and control of a robotic arm having four links. *Arab J Sci Eng*. 2017 May 1; 42(5): 1841–52. <https://doi.org/10.1007/s13369-016-2324-y>
74. Iqbal U, Samad A, Nissa Z, Iqbal J. Embedded control system for AUTAREP—A novel AUTonomous Articulated Robotic Educational Platform. *Tehnicki Vjesnik*. 2014 Dec 1; 21: 1255–61.
75. Manzoor S, Islam R, Khalid A, Samad A, Iqbal J. An open-source multi-DOF articulated robotic educational platform for autonomous object manipulation. *Robotics and Computer-Integrated Manufacturing*. 2014 Jun 1; 30(3):351–62. <https://doi.org/10.1016/j.rcim.2013.11.003>
76. KR QUANTEC [Internet]. KUKA AG. [cited 2022 Feb 1]. Available from: <https://www.kuka.com/en-de/products/robot-systems/industrial-robots/kr-quantec>